

TDC Model for PSG Sacrificial Layer Etching with Hydrofluoric Acid*

Wu Changju[†], Wang Hao, Jin Zhonghe, Ma Huilian, and Wang Yuelin

(Department of Information & Electronic Engineering, Zhejiang University, Hangzhou 310027, China)

Abstract: HF etching of sacrificial layers with different structures, namely channel, bubble, and joint-channel, is studied. The existing model cannot fit the experimental data well. The error of etching rate between the existing model and the experimental data increases with etching time. A modified model considering the diffusion coefficient as a function of HF concentration and temperature is proposed. The etching rate coefficient as a function of temperature and the effect of reaction production are also considered in the modified model. For the joint-channel structure, a new mathematical model for the etching profile is also adopted. Experimental data obtained with channel, bubble, and joint-channel structures are compared with the modified model and the previous model. The results show that the modified model matches the experiments well.

Key words: diffusion coefficient; etching rate; sacrificial oxide; TDC model

EEACC: 2520; 2575F

CLC number: TN304.12

Document code: A

Article ID: 0253-4177(2008)06-1094-09

1 Introduction

Sacrificial layer etching is a technology in which the sacrificial layer is selectively removed by etchant and a suspended structure is formed. It is widely used in the fabrication process of MEMS^[1]. The combination of HF and silicon dioxide or phosphosilicate-glass (PSG) is the most popular in sacrificial layer etching. Since over etching is harmful to the poly-silicon structure layer^[2], precise prediction of the etching process can not only improve the characteristics of MEMS devices but also save process time. Many reactive flux models have been proposed to predict the etching process, including the Deal-Grove model^[3], power law model^[4], langmuir-hinshelwood kinetics model^[5], and freundlich adsorption isotherm kinetics model^[6]. So far, the combined first-and-second order release-etching model presented by Monk^[2] and Liu *et al.*^[7] seems to predict the etching process well. Wu *et al.*^[8] use the power law model to predict the etching process. The results show that the model can also describe the etching process well. But compared to the combined first-and-second order model, the power law model is much more complex in solving the equations. In the model proposed by Monk^[2] and Liu *et al.*^[7], only the channel structure with an etching window at one end is considered. Eaton *et al.*^[9~11] extend the work done by Monk^[2] and Liu *et al.*^[7], making the etching model fit for not only simple structures (such as channel structure and bubble structure)

but also complex structures (such as join-channel structure) by applying different boundary conditions.

In the models proposed by Liu *et al.*^[7] and Eaton^[9~11], the diffusion coefficient of etchant is considered as a constant. Monk^[2] has proposed that the value of diffusion coefficient varies with the bulk etchant concentration. However, the diffusion coefficient is still assumed as a constant during the entire etching process for simplification. Since the assumption of constant diffusion coefficient of etchant is accepted in most existing models, these models will be referred to as constant diffusion coefficient models (CDC model) in the remainder of the paper. This assumption makes the models very simple. However, it may also cause error, especially for etching processes with a long etching time.

Secondly, in CDC model, all the etching experiments are done at a given room temperature and the etching rate coefficients are also obtained at that temperature. If the experiment temperature changes, the etching rate coefficients cannot be used again. There is no method proposed to calculate the etching rate coefficients at any temperature in the model.

Thirdly, in the CDC model, the effect of reaction production, namely H_2SiF_6 , is not considered for simplification. Whether the effect can be neglected or not requires further study.

Finally, for joint-channel structure, Eaton *et al.*^[9] proposed a model to calculate the etching rate. In his model, the etching front is assumed as a straight line when the etching front reaches the sec-

* Project supported by the National Basic Research Program of China (No.2006CB300405)

[†] Corresponding author. Email: wuchangju@zju.edu.cn

Received 13 January 2008, revised manuscript received 16 February 2008

ond channel. So the etching front area is equal to the section area of the second channel. The mathematic model proposed by Eaton *et al.* for joint channel structure works well when the etching starts from a wide channel, but it may be wrong when the etching starts from a narrow channel, because the etching front is no longer a straight line.

In this work, a modified model considering diffusion coefficient as a function of HF concentration and temperature is proposed. Accordingly, this modified model will be referred as the transformable diffusion coefficient (TDC) model. The etching rate coefficient as a function of temperature and the effect of reaction production are also considered in the TDC model. For joint-channel structure, a new mathematical model for the etching profile is proposed, which fits the experiments well. Experimental data obtained with channel, bubble, and joint-channel structures will be compared with the TDC model and the CDC model.

2 CDC model of sacrificial layer's etching

In the CDC model, the diffusion flux J_d , can be expressed as,

$$J_d = -D \frac{\partial C}{\partial x} = D \frac{(C_b - C)}{\delta} \quad (1)$$

where $\delta(t)$ is the etching front position, and C_b and C_s are the bulk concentration and HF concentration at etching front, respectively. D is the diffusion coefficient of HF solution. In the power law model^[4], the reactive flux is expressed as,

$$J_{HF} = kC^n \quad (2)$$

where n is the reaction order between 1 and 2, and k is the reaction coefficient. In the CDC model, J_{HF} is simplified as,

$$J_{HF} = k_1 C + k_2 C^2 \quad (3)$$

At steady state, the above fluxes are equal to each other,

$$J_d = J_{HF} \quad (4)$$

The etching rate is proportional to J_{HF} ^[7],

$$v = \frac{d\delta}{dt} = \frac{1}{6} \times \frac{M_{SiO_2}}{\rho_{SiO_2}} J_{HF} \quad (5)$$

where v is the etching rate, M_{SiO_2} molecular weight of SiO_2 , and ρ_{SiO_2} density of SiO_2 .

Equations (3), (4), and (5) are combined to yield,

$$\begin{aligned} \delta(t + \Delta t) &= \delta(t) + \frac{d\delta}{dt} \Delta t = \delta(t) + \\ &\frac{1}{6} \times \frac{M_{SiO_2}}{\rho_{SiO_2}} (k_1 C + k_2 C^2) \Delta t \end{aligned} \quad (6)$$

Equations (1), (3), and (4) are combined to yield,

$$C = \frac{-(k_1 \delta + D) + \sqrt{(k_1 \delta + D)^2 + 4k_2 \delta D C_b}}{2k_2 \delta} \quad (7)$$

According to Eqs. (6) and (7), the etching rate is a function of the diffusion coefficient D . In the CDC model, the value of D is measured by experiment at room temperature as $1.6 \times 10^{-5} \text{ cm}^2/\text{s}$. It is assumed to be constant throughout the entire etching process and at any temperature.

For bubble etching, a radical system is used. Then, Equation (1) becomes,

$$J_d = D \frac{C_b - C}{r(\ln r - \ln r_0)} \quad (8)$$

where r and r_0 are the radius of the etched disk and etching window, respectively. Other equations are the same as those of the channel structure.

For the joint-channel structure, when the etching reaches the joint, the diffusion flux of the second channel can be evaluated by applying a total mass flux boundary condition^[9].

$$J_1 S_1 = J_2 S_2 \quad (9)$$

where $J_{i(i=1,2)}$ and $S_{i(i=1,2)}$ are the diffusion flux and etching front area of the i th channel, respectively. The depth of the two channels is equal and marked with the letter H . So S_1 is the product of the W_1 (width of the first channel) and H . In Eaton's model, the etching front is assumed to be a straight line, so S_2 is the product of the W_2 (width of the second channel) and H .

3 TDC model of sacrificial layer's etching

3.1 Diffusion coefficient

In the CDC model, the diffusion coefficient D is considered as a constant. However, research in chemistry already indicates that the diffusion coefficient is a function of solution concentration and temperature^[12~14].

$$\begin{aligned} D(T) &= \frac{RT^2}{334\eta_w F^2} \times \frac{n_- + n_+}{n_- n_+} \times \frac{\lambda_+^0 \lambda_-^0}{\lambda_+^0 + \lambda_-^0} \left(1 - \frac{MC}{1000d}\right) = \\ &D_0(T) \left(1 - \frac{MC}{1000d}\right) \end{aligned} \quad (10)$$

where $D_0(T)$ and $D(T)$ are the diffusion coefficient at infinite dilution and at non-infinite dilution, λ_+^0 and λ_-^0 are the ions conductance, n_+ , n_- are the valences of cation and anion, F is faraday, η_w is the viscosity of water, C is the molar concentration of the solution, M_2 is the molecular weight of the solution, and d is the density of the solution. With the hydrofluoric acid, the values of λ_+^0 and λ_-^0 are 349.8 and 75 (A/cm²)(V/cm)(g-equiv/cm³)^[2] respectively. The absolute values of n_+ and n_- are both 1. M is the mo-

molecular weight of HF with a value of 20g/mol. Because the density of the solution is close to that of the water, it is assumed to be 1g/cm³ during the calculations.

3.2 Etching rate coefficients

Judge^[15] indicated that the etching rate coefficient could be expressed as,

$$k = A \exp^{-E_a/RT} \quad (11)$$

where k is the etching rate coefficient, A is a constant, E_a is the activation energy, and T is the temperature. For combined first-and-second order release-etching model, Equation (11) can be rewritten as,

$$k_{1,2} = A_{1,2} \exp^{-E_a/RT} \quad (12)$$

The activation energy for k_1 and k_2 are assumed equal to each other. Normally, activation energy is a function of the temperature. Since the temperature of measuring the activation energy and the temperature of sacrificial layer etching experiments are usually very close, the activation energy can be assumed to be a constant. The values of A_1 , A_2 , and E_a can be determined approximately by three experiments. The etching time for the three experiments should be very short, to make sure the diffusion-limited effect is ignorable. In this case, the HF concentration at the etching front is approximately equal to the bulk concentration. Therefore, the etching rate can be expressed approximately as,

$$v = \frac{1}{6} \times \frac{M_{\text{SiO}_2}}{\rho_{\text{SiO}_2}} (k_1 C_b + k_2 C_b^2) \quad (13)$$

For the three experiments, the temperature and solution concentration are set as (1) T_1, C_{b1} , (2) T_1, C_{b2} , and (3) T_2, C_{b1} . These will result in three different etching rate values. Using Eqs. (12) and (13), it is easy to calculate the values of E_a, A_1 , and A_2 .

In the following part, when a comparison between CDC model and TDC model is made, in order to make a fair comparison, the same k_1 and k_2 values obtained in this work are used for both the CDC model and TDC model during the calculation.

3.3 Effect of reaction production

In the CDC model, the effect of reaction production is not considered. Monk^[2] studied the effect of reaction production on the etching process. He found that the effect was small if the concentration of H_2SiF_6 in the solution was lower than 20% of HF concentration^[2]. So it will be helpful if we obtain the concentration of H_2SiF_6 at the reaction front. During the etching process, the reaction flow of H_2SiF_6 is 1/6 of the reaction flow of HF.

$$J_{\text{H}_2\text{SiF}_6} = \frac{1}{6} J_{\text{HF}} \quad (14)$$

At steady state, the reaction flux should be equal

to diffusion flux,

$$J_{\text{H}_2\text{SiF}_6} = J_D \quad (15)$$

Assuming the linear distribution of H_2SiF_6 concentration,

$$J_D = D_{\text{H}_2\text{SiF}_6} \times \frac{C_{\text{H}_2\text{SiF}_6} - C_{b(\text{H}_2\text{SiF}_6)}}{\delta} \quad (16)$$

where $D_{\text{H}_2\text{SiF}_6}$ is the diffusion coefficient of H_2SiF_6 with the value $7.7 \times 10^{-6} \text{cm}^2/\text{s}$ according to Monk^[2], $C_{\text{H}_2\text{SiF}_6}$ is the concentration of H_2SiF_6 at the etching front, and $C_{b(\text{H}_2\text{SiF}_6)}$ is the bulk concentration outside the reaction channel. Since the reaction product is very small compared with the total solution used for etching, it is reasonable to consider $C_{b(\text{H}_2\text{SiF}_6)}$ as 0. Therefore,

$$J_{\text{H}_2\text{SiF}_6} = 6 D_{\text{H}_2\text{SiF}_6} \frac{C_{\text{H}_2\text{SiF}_6}}{\delta} = k_1 C + k_2 C^2 \quad (17)$$

The concentration of H_2SiF_6 can be obtained with Eq. (17).

3.4 Etching front area

In Eaton's model, the etching front is assumed as a straight line for the whole etching process^[9]. So the etching front area S_2 in Eq. (9) is equal to the section area of the second channel, i.e. $W_2 H$. This is true for the etching process in the wide-narrow channel. However, if the etching process starts from the narrow channel, the etching front presents an arc rather than a straight line when the etching front reaches the wide channel. In this case, the etching front area S_2 depends on the profile of the etching front.

Through many experiments with a narrow-wide structure, Wu *et al.*^[16] found the shape of the etching front can be simplified as an arc. The radius of the arc can be calculated as,

$$r = \begin{cases} x + \frac{W_1}{2} + \frac{W_1^2}{8x}, & x \leq \frac{W_2 - W_1}{2} \\ x + \frac{W_1}{2} + \frac{W_1^2}{4(W_2 - W_1)}, & x > \frac{W_2 - W_1}{2} \end{cases} \quad (18)$$

Then, S_2 can be expressed as,

$$S_2 = \begin{cases} \frac{r\pi H}{90} \sin^{-1} \left(\frac{x + W_1/2}{r} \right), & x \leq \frac{W_2 - W_1}{2} \\ \frac{r\pi H}{90} \sin^{-1} \left(\frac{W_2}{2r} \right), & x > \frac{W_2 - W_1}{2} \end{cases} \quad (19)$$

The etching front area is different from $W_2 H$ as indicated by Eq. (19). However, as the etching process proceeds, the etching front becomes a straight line and the area is close to $W_2 H$ again. This can be seen more clearly in the calculated results in the results and discussion.

For wide-narrow structure, i.e., $W_1 > W_2$, $S_2 = W_2 H$.

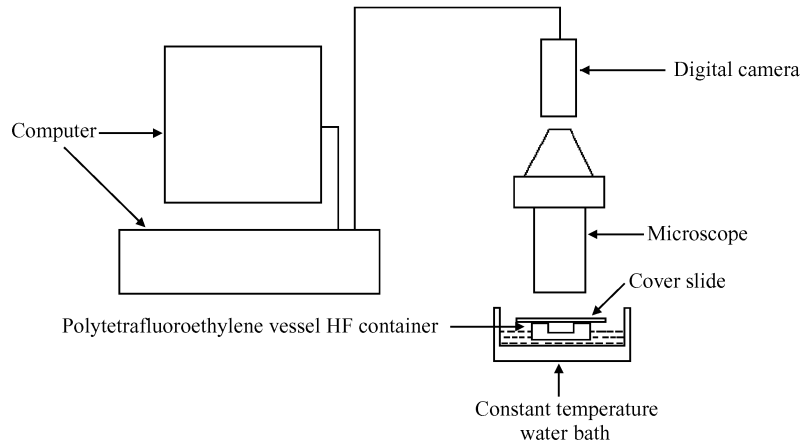


Fig. 1 Schematic of the experimental setup

The final equations for the TDC model and CDC model are,

$$\left\{ \begin{aligned} \frac{d\delta(i)}{dt} &= \frac{1}{6} \times \frac{M_{SiO_2}}{\rho_{SiO_2}} (k_1 C(i-1) + k_2 C(i-1)^2) \\ \delta(i) &= \delta(i-1) + \frac{d\delta(i-1)}{dt} \Delta t \\ D(i) &= D_0(T) \left(1 - \frac{MC(i-1)}{1000d} \right), \text{ for TDC model} \\ D(i) &= 1.6 \times 10^{-5} \text{ cm}^2/\text{s}, \text{ for CDC model} \\ C(i) &= \frac{-(k_1 \delta(i-1) + D(i))}{2k_2 \delta(i-1)} + \\ &\frac{\sqrt{(k_1 \delta(i-1) + D(i))^2 + 4k_2 \delta(i-1) D(i) C(i-1)}}{2k_2 \delta(i-1)} \end{aligned} \right. \quad (20)$$

where $i = 1, 2, 3, \dots$. At the initial time, C is equal to C_b , i.e., $C(0) = C_b$. For the CDC model, the $D(i)$ is assumed to always equal $1.6 \times 10^{-5} \text{ cm}^2/\text{s}$.

4 Experiment

The process to fabricate the samples begins with a 4-inch silicon wafer. First, a PSG layer is deposited on silicon by low-pressure chemical vapour deposition (LPCVD). The PSG layer is patterned to form the island followed by deposition of an LPCVD low-stress polysilicon structural layer. Finally, etching windows are opened by plasma etching. The samples include channel structure, bubble structure, and joint-channel structure. The width of the channel is $200 \mu\text{m}$ and the etching window is equal to the width. For the bubble structure, an etch window with the radius of 5, 10, or $20 \mu\text{m}$ is at the center of the bubble. For the join-channel structure, the two channels are 20 and $160 \mu\text{m}$, respectively.

A polytetrafluoroethylene vessel with hydrofluoric acid covered with a plastic cover slide is put in the bath for enough time to ensure the temperature of the etchant is the same as that of the bath. The cover

slide is used to reduce the volatilization of HF and to avoid the mixing of the HF and water vapor. Then the sample is put into the vessel to begin the etching process. The etching process can be monitored by a camera through a microscope in real time. The etched length can be read out from the ruler in the etched sample and the photo will be taken by a digital camera. Figure 1 is the schematic of the experimental setup, including the water bath, digital camera, microscope and computer.

5 Results and discussion

5.1 Effect of HF concentration on the etching rate

The effect of concentration on the etching rate with channel structure is shown in Fig. 2 and Fig. 3. The concentrations of HF solution are 24, 16, and 12 mol/L , respectively. The temperature is 25°C . The etching rate of the experiment is obtained by the difference between the neighbor data of etching length.

Figure 2 shows that the etching length increases with the etching time for all HF concentrations. For the same etching time, the etching length is larger in higher HF concentrations. Figure 3 shows that the

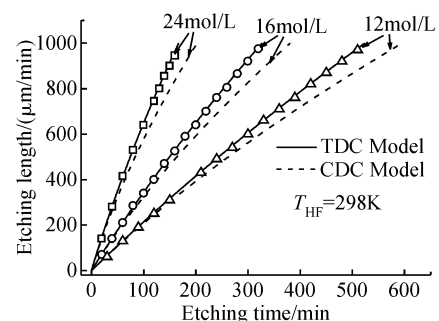


Fig. 2 Etching length as a function of etching time with different HF concentrations

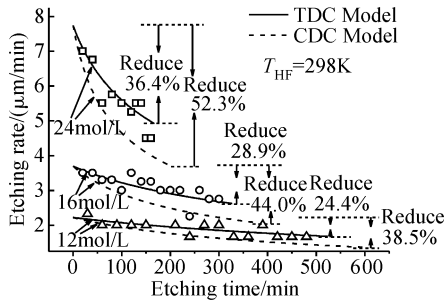


Fig. 3 Etching rate as a function of etching time with different HF concentrations

calculated initial etching rate is 7.74, 3.70, and 2.22 $\mu\text{m}/\text{min}$ for 24, 16, and 12 mol/L HF solution, respectively, for both the CDC model and TDC model. For the three HF concentrations, the etching rate decreases with etching time, as shown in Fig. 3. This can be explained by the etchant concentration at the etching front decreasing gradually during the etching process because of diffusion limitation. It is not surprising that the etching rate decreases more quickly in higher concentrations of HF solution since the diffusion limitation is more evidence in higher concentration solutions.

After etching of 1000 μm , the CDC model indicates that the etching rates decrease to 3.69, 2.07, and 1.37 $\mu\text{m}/\text{min}$, which are 47.7%, 56.0%, and 61.5% of the initial etching rates in 24, 16, and 12 mol/L HF solution, respectively. But both the experiments and the TDC model indicate that the etching rates do not decrease as seriously as predicted by the CDC model. The etching rates at length of 1000 μm are 4.92, 2.63, and 1.68 $\mu\text{m}/\text{min}$, which are 63.6%, 71.1%, and 75.6% of the initial rates for 24, 16, and 12 mol/L, respectively. The rates obtained by the TDC model are 33.3%, 27.1%, and 22.6% higher than those by the CDC model when the etching length reaches 1000 μm for 24, 16, and 12 mol/L, respectively.

As indicated by Fig. 2, both models match well the initial 200 μm etching process for all HF concen-

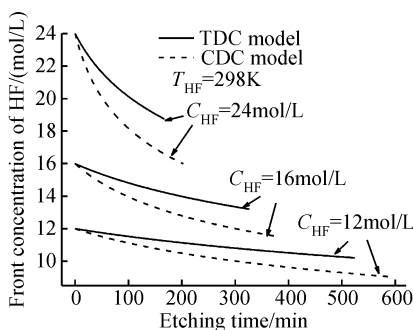


Fig. 4 Front concentration of HF calculated by the TDC model and the CDC model

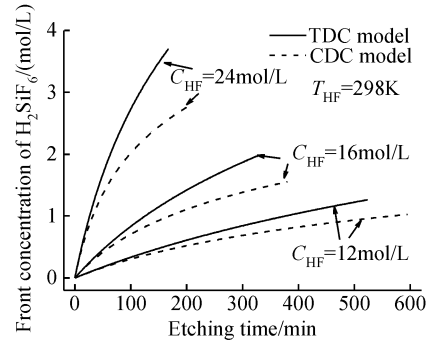


Fig. 5 Front concentration of H_2SiF_6 calculated by the TDC and the CDC model

trations. But for the extended etching process, the difference between the CDC model and the experimental data is obvious, while the TDC model still matches the experimental data well. The etching length and rate obtained by the CDC model are less than those obtained by experiments. The error of the CDC model increases with etching time and initial HF concentration. The error of length reaches as high as 13.6% for the 1000 μm etching process at 24 mol/L HF solution. But the difference between the TDC model and the experimental data is less than 4.8%.

5.2 Effect of reaction production on the etching rate

Calculated using Eqs. (17) and (20) for the TDC model and the CDC model, the concentrations of H_2SiF_6 and HF at the etching front as functions of the etching time are shown in Fig. 4 and Fig. 5.

The diffusion coefficient of HF at the etching front calculated by the CDC model and the TDC model is shown in Fig. 6. The ratio of front concentration of H_2SiF_6 and HF is shown in Fig. 7. For both models, the HF concentration decreases with etching length, resulting in the etching rate decreasing during the extended etching process as shown in Fig. 4. On the other hand, the diffusion coefficient increases with the decrease of the HF concentration, as indica-

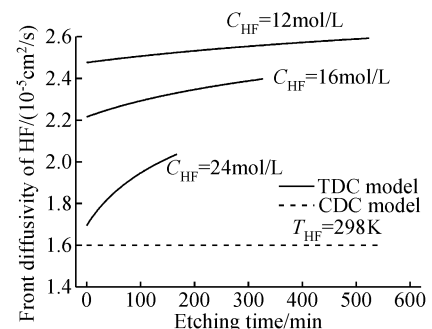


Fig. 6 Front diffusivity of HF calculated by the TDC model and the CDC model

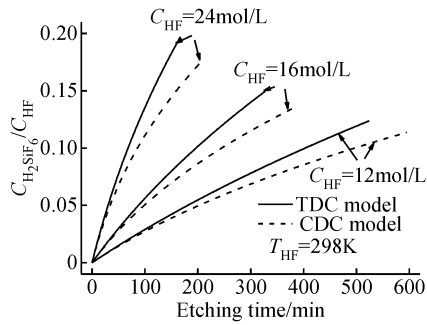


Fig. 7 Ratio of front concentration of H_2SiF_6 and HF calculated by the TDC and the CDC model

ted by Eq. (10) for the TDC model. For the etching processes with 12, 16, or 24 mol/L, the diffusion coefficient increases from 2.48×10^{-5} to 2.59×10^{-5} , from 2.22×10^{-5} to $2.40 \times 10^{-5} \text{ cm}^2/\text{s}$, or from 1.69×10^{-5} to $2.04 \times 10^{-5} \text{ cm}^2/\text{s}$, respectively. So the etchant can diffuse to the etching front more quickly during the etching process, resulting in the concentration decreasing more slowly than the prediction of the CDC model. In this way, increasing the diffusion coefficient partly compensates the diffusion limitation during the extended etching. The higher the bulk etchant concentration, the more obvious the effect of compensation is. In the CDC model, the diffusion coefficient is considered as constant for different HF concentrations. So the etchant concentration at the etching front in the CDC model drops more quickly than that in the TDC model.

The concentrations of the reaction product, namely H_2SiF_6 , increase both with the etching time and with the HF bulk concentration. But the ratio of front concentration of H_2SiF_6 and HF is lower than 20% for all the etching processes, as shown in Fig. 7. So it is acceptable to neglect the effect of the etching product. If the etching length becomes longer, the H_2SiF_6 concentration will increase to above 20% of the HF concentration for 24 mol/L HF solution. At that time, a more complex diffusion model should be used.

5.3 Effect of temperature on the etching rate

The etching length and etching rate as functions of etching time at different temperatures are shown in Fig. 8 and Fig. 9, respectively. The temperatures are 27 and 17°C, respectively. The concentration of the HF solution is 20 mol/L. The higher the temperature, the quicker the initial etching rate is. This is reasonable since the reaction coefficients, k_1 and k_2 , are proportional to temperature. On the other hand, the error between the CDC model and the experimental data is higher at higher temperatures. For example, when the temperature is 27°C, the end etching rate is $4.05 \mu\text{m}/$

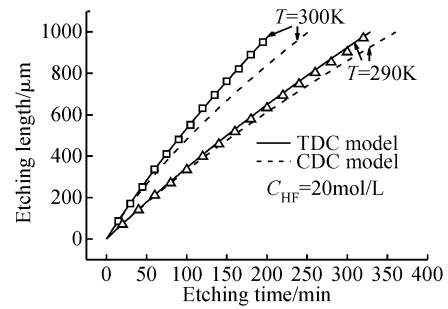


Fig. 8 Etching length as a function of etching time with different temperatures

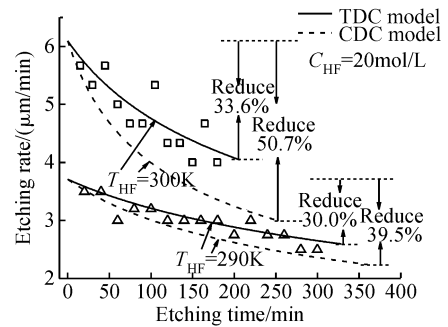


Fig. 9 Etching rate as a function of etching time with different temperatures

min and $3.00 \mu\text{m}/\text{min}$, respectively, for the TDC model and CDC model. The error is 35.0%. When the temperature is 17°C, the end etching rate is 2.60 and $2.24 \mu\text{m}/\text{min}$, respectively, for the two models. The error is 16.1%. This again is because the CDC model considers the diffusion coefficient constant at different temperatures.

5.4 Effect of etching hole on the etching rate

The etching behavior of the bubble structure is similar to that of the channel structure. Moreover, the etching rate of the bubble structure is related with the size of the etching hole. The etching rate as a function of etching time with different etching holes is shown in Fig. 10. The radius of the etching hole is 5, 10, or

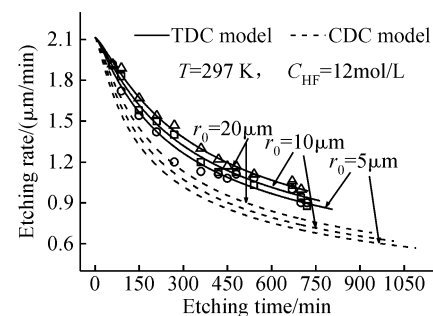


Fig. 10 Etching rate as a function of etching time with different etching holes

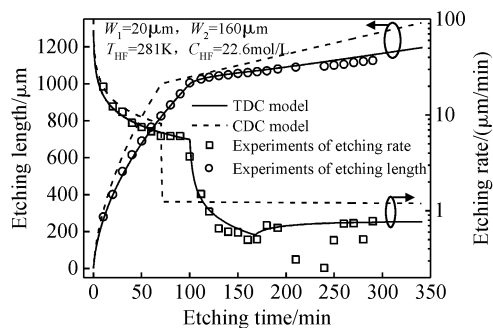


Fig.11 Etching length and rate as functions of etching time with the TDC model, CDC model, and experiments. Widths of the first channel and second channel are 20 and 160 μm , respectively. The HF concentration is 22.6 mol/L. The temperature is 281K.

20 μm , respectively. The initial etching rate is the same, namely 2.11 $\mu\text{m}/\text{min}$ with different radii of the etching hole. When the etching length reaches 700 μm , the etching rate in the TDC model is 0.907, 0.951, and 1.00 $\mu\text{m}/\text{min}$ with the etching hole of 5, 10, and 20 μm , respectively. For the CDC model, when the etching length reaches 700 μm , the etching rate by the CDC model is 0.701, 0.738, and 0.782 $\mu\text{m}/\text{min}$, respectively. When the etching hole becomes larger, the amount of etchant flowing into the etching hole increases. Then, the diffusion limited is relative small. Therefore, the etching rate increases with the radius of the etching hole. On the other hand, it seems that the larger the etching hole, the smaller the differences between the TDC model and CDC model. For example, the relative error between TDC model and CDC model is 29.4%, 28.7%, and 28.0%, respectively. Although the etching rate increases with radius of the etching hole, the difference between C_s and C_b decreases with the increase of the radius. Therefore, the error of the diffusion coefficient used in the CDC model decreases, resulting in the error of etching rate decreasing with the increase of the radius.

5.5 Effect of etching front on the etching rate

The etching length and rate as functions of etching time for the narrow-wide channel is shown in Fig. 11. The etching process begins from a narrow channel with a width of 20 μm , which is connected with a wide channel with a width of 160 μm . The lengths of the narrow and wide channels are 1000 and 500 μm , respectively. The temperature is 281K. The HF concentration in the etching solution is 22.6 mol/L. As shown in Fig. 11, the etching process can be separated into 4 stages, (1) the first 1000 μm , (2) 1000 ~ 1070 μm , (3) 1070 ~ 1254 μm , and (4) the final 246 μm . The results are similar to the work published in Ref. [16], in which the etching process can also be separa-

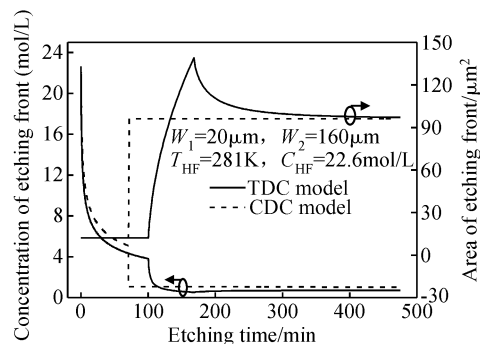


Fig.12 Concentration and area of the etching front as functions of etching time with the TDC model, CDC model, and experiments. Widths of the first channel and second channel are 20 and 160 μm , respectively. The HF concentration is 22.6 mol/L. The temperature is 281K.

ted into 4 stages. In Ref. [16], the width ratio is 4, with the widths of the narrow channel and wide channel are 25 and 100 μm , respectively. In this work, the width ratio is 8. For narrow-wide joint channels, the etching process is similar though the width ratio is different.

As indicated by Ref. [16], during the first 1000 μm of etching, the etching length increases with the etching time quickly, according to the experiment and both models. The initial etching rate is about 77.0 $\mu\text{m}/\text{min}$ for both models. After 20 min of etching, the etching rate predicted by the CDC model is significantly larger than that by the experiment. With the CDC model, the first 1000 μm can be etched in 70.6 min. However, the actual time is 99.9 min according to the experiment. The difference reaches above 40%. The etching time predicted by the TDC model is 100.1 min for the first 1000 μm . The error of etching time predicted by the TDC model is less than 0.2%.

In this stage, the etching rate decreases quickly. According to CDC model, the etching rate at the end of the first 1000 μm is about 8.1 $\mu\text{m}/\text{min}$, which is about 10.5% of the initial etching rate. However, this rate is still much higher than that predicted by the TDC model. With the TDC model, the etching rate at the end of the first 1000 μm is about 4.89 $\mu\text{m}/\text{min}$. This is only about 6.35% of the initial etching rate. The decrease of the etching rate indicates the decrease of HF concentration at the etching front, as shown in Fig. 12. For example, the front concentration decreases from 22.6 to 5.08, or 3.81 mol/L, according to the CDC model or the TDC model, respectively. Compared with Ref. [16], the results are the same in this stage. This shows that the etching behavior is independent of the width in a single channel structure. The same phenomenon is also observed by Liu^[7].

In the second stage, the etching rate decreases suddenly in a very short time. For the CDC model, this is mainly due to the etching front area increasing suddenly from 12 to $96\mu\text{m}^2$ as shown in Fig. 12. For the TDC model, the etching front presents an arc at the beginning of the second channel, and the etching front area increases gradually as shown in Fig. 12. The etching front area at this stage increases from 12 to $96\mu\text{m}^2$ and further to $139\mu\text{m}^2$. The etching front area can be larger than the cross section area of the channel, since the etching front is an arc. The area increases to 11.58 times the initial $12\mu\text{m}^2$, resulting in the HF concentration decreasing from 3.81 to 0.51mol/L . This further results in the etching rate decreasing gradually from 4.89 to $0.57\mu\text{m}/\text{min}$ in 68min. At this time, the etching length is about $1070\mu\text{m}$. In this stage, the end etching rate is lower than in Ref. [16], which is $1.01\mu\text{m}/\text{min}$. The total etching time is longer than in Ref. [16], which is 19min. This is because the larger the width ratio, the more obvious the diffusion limitation is. Furthermore, the maximal area of etching front also increases with the width ratio. This may also result in the increase of the etching time.

For the CDC model, the etching rate decreases gradually, as in the first channel. But for the TDC model, the situation is much more complex. The following etching process can also be divided into two stages. In the two stages, the etching front area decreases gradually from 139 to $96\mu\text{m}^2$ again. In the third stage, the etching rate will increase slightly, much different from the CDC model. At 415.5min in Fig. 11, the etching rate reaches the maximum $0.77\mu\text{m}/\text{min}$, which is 35.1% higher than the minimum value, $0.57\mu\text{m}/\text{min}$ at the second channel. At this time, the etching front area decreases to $97.5\mu\text{m}^2$, and the etching length reaches $1254\mu\text{m}$. After that, the etching process goes into the 4th stage. In this stage, the etching front tends to a straight line and the etching front area tends to $96\mu\text{m}^2$. At the end of the total $1500\mu\text{m}$ etching length, the etching rate decreases to $0.76\mu\text{m}/\text{min}$, which is 1.30% lower than the maximum value of $0.77\mu\text{m}/\text{min}$.

The TDC model matches the experimental data much better than CDC model, as shown in Fig. 11.

Although the same k_1 and k_2 are used for the two models in this work, the etching rate by CDC model is larger than that by the TDC model for the joint channel structure, as shown in Fig. 11, but smaller than that by TDC model for channel structure as shown in Fig. 2 and Fig. 3 for the bubble structure as shown in Fig. 10. This is mainly due to the diffusion coefficient used in the CDC model. In the CDC model, D is a constant and the value used is measured by experi-

ments at room temperature, i.e. about 20°C . So for the joint channel structure, the diffusion coefficient used in the CDC model is much larger than that in the TDC model, as the process temperature is 8°C . For channel structure and bubble structure, the process temperature is 25 and 24°C , respectively. Then, the diffusion coefficient used in CDC model is smaller than that in the TDC model.

6 Summary

The sacrificial layer etching model with different structures is studied with HF etching of PSG as an example. The CDC model considers the diffusion coefficient D as constant during the entire etching process. However, it is found that this model cannot predict the extended etching process accurately, especially at temperatures different from room temperature. The error of the etching rate of this model can reach higher than 30% during extended etching. This work obtains the diffusion coefficient of HF as a function of solution concentration and temperature. It is found the diffusion coefficient increases with the decrease of the etchant concentration. Increasing temperature also causes an increase of the diffusion coefficient. Thus, a modified model named the TDC model is proposed. The TDC model matches the experiments well. The effect of the reaction product is also analyzed.

The etching of SiO_2 or related mixed oxides is a complicated reaction. The reactive species that attacks the oxide is HF_2^- , a complex ion that is formed by the presence of F^- ions and HF molecules. To simplify the model, only HF is considered in this work for the etching and diffusion process. Fortunately, the error of the etching length predicted by the modified model is less than 5%, which is acceptable in most cases. As etching length increases further, the effect of etching products will affect the etching and diffusion process seriously. In that case, more a complicated model may be necessary for accurate predictions.

Acknowledgements The authors would thank the Institute of Microelectronic at Beijing University, Shanghai Institute of Microsystems and Information Technology, and Micro-fabrication Facility (MFF) at Hong Kong University of Science and Technology, for the fabrication of the samples.

References

- [1] Teh W H, Liang C T, Graham M, et al. Cross-linked PMMA as a low-dimensional dielectric sacrificial layer. *J Microelectromechan Syst.* 2003, 12(5):641
- [2] Monk D J. Controlled structure release for silicon surface mi-

- cromachining. PhD Dissertation, California University at Berkeley, 1993
- [3] Jaeger R C. Introduction to microelectronic fabrication. Addison-Wesley Publishing Company, 1990
- [4] Blumberg A A, Stravrinou S C. Tabulated functions for heterogeneous reaction rates; the attack of vitreous silica by hydrofluoric acid. *J Phys Chem*, 1960, 64: 1438
- [5] Kline W E, Fogler H S. Dissolution of silicate minerals by hydrofluoric acid. *Industrial and Engineering Chemistry Fundamentals*, 1981, 20: 155
- [6] Fogler H S, Lund K, McCune C C. Acidization-III: the kinetics of the dissolution of sodium and potassium feldspar in HF/HCl acid mixtures. *Chemical Engineering Science*, 1975, 30: 1325
- [7] Liu J Q, Tai Y C, Lee J, et al. In situ monitoring and universal modeling of sacrificial PSG etching using hydrofluoric acid. *Proc IEEE, MEMS'93*, 1993: 71
- [8] Wu C J, Ma H L, Jin Z H, et al. A modified model for the etching of a sacrificial layer in bubble structures. *Chinese Journal of Semiconductors*, 2006, 27(1): 183
- [9] Eaton W P, Smith J H, Jarecki R L. Release-etch modeling for complex surface micromachined structures. *Proceeding of the SPIE*, 1996, 2879: 80
- [10] Eaton W P, Jarecki R L, Smith J H. Prediction of release-etch times for surface-micromachined structures. 1997 International Conference on Solid State Sensors and Actuators (TRANSDUCERS'97), 1997, 1: 249
- [11] Eaton W P. Surface micromachined pressure sensors. PhD Dissertation, University of New Mexico, 1997
- [12] Reid R C, Prausnitz J M, Poling B E. The properties of gases & liquids. New York: McGraw-Hill, 1986
- [13] Gordon A R. The diffusion of an electrolyte, and its relation to concentration. *J Chem Phys*, 1937, 5: 522
- [14] Harned H S, Owen B B. The physical chemistry of electrolytic solutions. New York: Reinhold Publishing Corporation, 1950
- [15] Judge J S. The etching of the film dielectric materials. *Proceedings of the Symposium on Etching for Pattern Definition*, Princeton, New Jersey, The Electrochemical Society, 1976: 19
- [16] Wu C J, Jin Z H, Ma H L, et al. Sacrificial layer etching in joint channels. *Journal of Micromechanics and Microengineering*, 2006, 16(11): 2323

氢氟酸和 PSG 牺牲层腐蚀的 TDC 模型*

吴昌聚[†] 王 昊 金仲和 马慧莲 王跃林

(浙江大学信息与电子工程系, 杭州 310027)

摘要: 对不同结构,即直沟道结构、冒泡结构和组合沟道结构的氢氟酸牺牲层腐蚀进行了研究.以往的牺牲层腐蚀模型和实验结果不能很好地吻合.以往的模型和实验结果的误差随着腐蚀时间的增加而增大.本文提出了一个修正模型,在修正模型中:HF的扩散系数是浓度和温度的函数;腐蚀速率常数是温度的函数;此外还考虑了腐蚀产物对腐蚀过程的影响.对于组合沟道结构,对腐蚀前端形状的描述采用了一个新的数学模型.实验结果和以往的模型以及修正模型进行了对比,结果表明修正模型能够和实验结果吻合得很好.

关键词: 扩散系数; 腐蚀速率; 牺牲层; TDC 模型

EEACC: 2520; 2575F

中图分类号: TN304.12

文献标识码: A

文章编号: 0253-4177(2008)06-1094-09

* 国家重点基础研究发展规划资助项目(批准号:2006CB300405)

[†] 通信作者. Email: wuchangju@zju.edu.cn

2008-01-13 收到, 2008-02-16 定稿